Charge Transfer through Single-Stranded Peptide Nucleic Acid Composed of Thymine Nucleotides

Amit Paul,[†] Richard M. Watson,[‡] Paul Lund,[‡] Yangjun Xing,[§] Kathleen Burke,[‡] Yufan He,[§] Eric Borguet,*[,§] Catalina Achim,*[,‡] and David H. Waldeck*[,†]

Department of Chemistry, University of Pittsburgh, Pittsburgh, Pennsylvania 15260; Department of Chemistry, Carnegie Mellon University, Pittsburgh, Pennsylvania 15213; and Department of Chemistry, Temple University, Philadelphia, Pennsylvania 19122

Received: December 14, 2007; In Final Form: February 18, 2008

Self-assembled monolayers (SAMs) of single-stranded peptide nucleic acids (PNAs) containing 3 to 7 thymine (T) nucleotides, a C-terminus cysteine, and an N-terminus ferrocene group were formed on gold electrodes. The existence of two redox environments for the ferrocene was detected by cyclic voltammetry and was attributed to the presence of "lying-down" and "standing-up" PNA molecules. By exploiting the chemical instability of the ferrocenium ion, electrochemical cycling was used to destroy the ferrocene of "lying-down" molecules while keeping the ferrocene in the "standing-up" molecules intact. Electrochemical measurements were used to determine the electron-transfer rate through the "standing-up" PNA molecules. The tunneling decay constant for these SAMs was determined to be about 0.9 $Å^{-1}$.

Introduction

The interest in self-assembled monolayers (SAMs)[1,2] of nucleic acids has increased recently, largely because of their potential applications in molecular electronics,[3] materials science,[4] molecular recognition,[5] biotechnology, and biosensor development.[6−8] An understanding of the charge transport (CT) through such SAMs is needed to realize their potential in molecular electronics and biosensing. The past decade has seen progress in understanding charge transfer through deoxyribonucleic acid (DNA), which is believed to occur through either a superexchange mechanism,[9−19] which dominates at short distances, or a hopping mechanism,[20−25] which dominates at large distances.

The weak distance dependence of the charge hopping mechanism and its prevalence in duplex DNA systems have motivated the exploration of charge transfer through DNA and its promise for molecular electronics by a large number of different research groups. Nevertheless, only a few research groups have studied CT in DNA monolayers, probably because of the difficulties in creating well-defined DNA assemblies on a metal surface.[26−28] For example, Hartwich et al.[29] used cyclic voltammetry to characterize charge transfer in mixed monolayers of DNA having a pyrroloquinoline−quinone redox probe attached to DNA through a spacer and linked to an Au(111) surface through an ethane−thiol linker. These studies determined that the CT rate constant for a 12-base-pair (bp) DNA duplex was 1.5 s^{-1}, while for the same duplex containing two mismatches it was 0.6 s^{-1}, and that charge transfer could not be detected for single-stranded (ss) DNA at a scan rate of >10 mV s^{-1}. Liu et al.[30] argued that CT through a monolayer of a 30-bp double-stranded (ds) DNA takes place through the nucleobase stack and does not involve the DNA backbone. They based their argument on the fact that the rate constant for CT of 30 s^{-1} was not affected by breaks in the sugar−phosphate backbone and was too small to be measured when a mismatch was introduced in the ds DNA. Interestingly, a similar rate constant for CT was measured for a monolayer of a 15-bp ds DNA.[31] CT rate constants for ss oligonucleotides are also quite high. For example, Kraatz and collaborators reported a CT rate constant of 12 s^{-1} for a 20-base ss DNA monolayer, which was only 10 times lower than the rate constant for a monolayer of the corresponding 20-bp ds DNA.[32,33] The studies on duplex DNA indicate an important role for the base pairs in CT, and those on ss-DNA suggest that the bases may contribute significantly even when they are not involved in base pairing.

Peptide nucleic acid (PNA) is an analogue of DNA that has a neutral and achiral backbone based on aminoethylglycine, in contrast to the negatively charged and chiral backbone of DNA (Figure 1a).[34,35] Like DNA, PNA forms duplexes with itself and other nucleic acids by Watson−Crick base pairing. The PNA·PNA duplexes adopt a helical structure termed P-type, which has a large pitch with 18 bases/turn, diameter of 28 Å, and 3.2−3.4 Å rise/base pair.[36−38] Recent work shows that ligand-modified PNA can be used as a scaffold for transition metal ions.[39−41] The inorganic nucleic acid structures formed by this method contain transition metal ions at specific positions and may mediate CT over tens of nanometers, in a manner similar to that in which metal cofactors mediate electron transfer in metalloproteins. The study of charge transfer in such metalized PNA is a long-term goal toward which the experiments described below are targeted.

ssPNA has a clear advantage over ssDNA for SAM preparation because it is neutral.[42−44] Martin-Gago and co-workers[42−44] successfully prepared SAMs of ss PNA molecules having a cysteine group at the C-terminus that bound the PNA to the gold surface. They characterized the surface by X-ray photoemission spectroscopy (XPS), atomic force microscopy (AFM), X-ray absorption near-edge spectroscopy (XANES), and reflection−absorption infrared spectroscopy (RAIRS). They proposed that the formation of PNA SAMs occurs in two main steps; at low coverage, the adsorbed ss PNA molecules lie down on the surface; as the surface coverage increases, the layer of lying

* To whom correspondence should be addressed.
[†] University of Pittsburgh.
[‡] Carnegie Mellon University.
[§] Temple University.

10.1021/jp711764q CCC: $40.75
Published on Web 04/16/2008

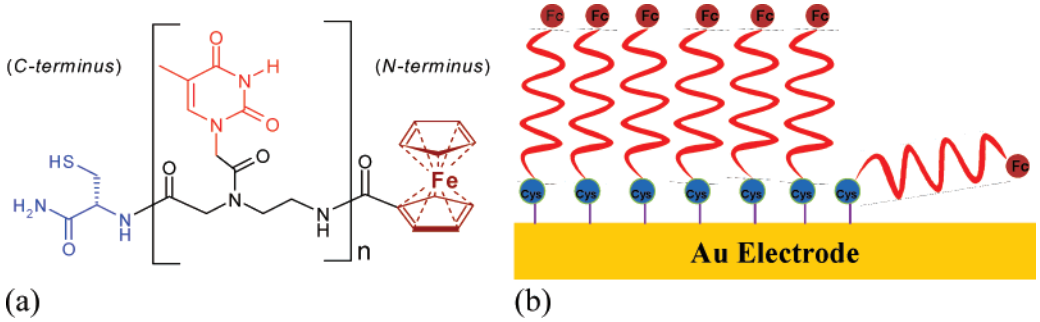

Figure 1. (a) Chemical structure of thymine containing ss PNA that has a C-terminus cysteine and an N-terminus ferrocene, where $n = 3-7$. (b) Panel B shows a schematic representation of PNA molecules self-assembled on a gold surface, in which the blue circle represents cysteine, the red curl represents PNA, and the light brown circle represents ferrocene.

down molecules undergoes a phase transition and the PNA realigns perpendicular to the surface. This two-phase mechanism is similar to that proposed for the formation of alkanethiol SAMs.[1,2]

In this work, PNA SAMs were grown on gold ball electrodes and used to systematically study the distance dependence of the electron transfer to a ferrocene redox reporter. The changeover of mechanism from tunneling to hopping in DNA has been shown to depend on the bases present in the nucleic acid and is linked to their oxidation potential.[20] Among the four different natural nucleobases, thymine (T) and cytosine have the highest oxidation potential.[45] Therefore, the changeover from a superexchange mechanism to charge hopping in T-only nucleic acids should occur at larger distances than for nucleic acids composed of other nucleobases. With an aim to evaluate electron tunneling in PNA-based SAMs, the electron transfer through short PNA oligomers containing thymine only were studied (see Figure 1a). PNA was immobilized on a gold surface through a cysteine group at the C-terminus of the PNA (Figure 1b), which forms a gold−sulfur bond. A ferrocene redox probe was covalently attached at the N-terminus of the PNA. The presence of two distinct subpopulations of the ferrocene, namely a fast CT rate, or "lying-down", population and a slow CT rate, or "standing-up", population was detected by atomic force microscopy (AFM) and cyclic voltammetry (CV). This finding was supported by ellipsometry[46,47] and contact angle studies. By electrochemically destroying the fast population, it was possible to measure the electron-transfer rate constants for the slow population. The length of the PNA was varied by increasing the number of thymine nucleotides, and the tunneling decay constant (β) for single-stranded PNA molecules was determined. The rapid decay of the charge-transfer rate with increasing number of thymines was found to be consistent with a superexchange-mediated tunneling mechanism.

Experimental Section

PNA Synthesis. PNA oligomers were synthesized by solid-phase peptide synthesis using the Boc protection strategy.[48−50] MBHA resin (Peptides International, Louisville, KY) with a loading of 0.18 mequiv/g was downloaded (see ref 50 for more details about this procedure) using Boc-L-Cys-(4-MeOBzl)-OH (NovaBiochem/Merck Biosciences, Switzerland) to an estimated loading of 0.04−0.06 mequiv/g. Thereafter, 3−7 Boc-T-OH PNA monomers (Applied Biosystems, Foster City, CA) were coupled using *O*-(1*H*-6-chlorobenzotriazole-1-yl)-*N*,*N*,*N*′,*N*′-tetramethyluronium hexafluorophosphate (HCTU, Peptides International) or *O*-benzotriazoly-1-yl-*N*,*N*,*N*′,*N*′-tetramethyluronium hexafluorophosphate (HBTU, Peptides International) as a coupling agent. Finally, ferrocenecarboxylic acid (Aldrich) was coupled to the N-terminus using the same coupling procedure, repeated twice to increase the yield of ferrocene-conjugated PNA. Oligomers were cleaved from the resin using solutions of trifluoroacetic acid (TFA), trifluoromethanesulfonic acid (TFMSA), thioanisole, and *m*-cresol, precipitated in ethyl ether, and dried under nitrogen. The solid products were dissolved in 15% acetonitrile aqueous solution and purified by reverse-phase HPLC using a solvent gradient, from 15% to 35% acetonitrile in water with 0.1% TFA over 40 min on a Waters Delta 600 pump with a 2996 photodiode array detector (Milford, MA). PNA oligomers were characterized by MALDI-TOF mass spectrometry on an Applied Biosystems Voyager-DE STR workstation (MALDI-TOF mass spectrograms are available in the Supporting Information).

TABLE 1: Incubation Temperature and Incubation Time Used for PNA SAM Preparation

molecule	temp (°C)	incubation time (h)
Cys-T3-Fc	40	40
Cys-T4-Fc	35/40	40
Cys-T5-Fc	40	40
Cys-T6-Fc	40	40
Cys-T7-Fc	40	28

PNA solutions were prepared in deionized water and the PNA concentrations were determined by UV−vis spectrophotometry at 95 °C assuming $\epsilon_{260} = 8600\ \text{cm}^{-1}\ \text{M}^{-1}$ for each T monomer.[50] PNA solutions for electrode incubation were typically 20 μM ssPNA in 10 mM pH 7.0 sodium phosphate buffer solution that was a 50% acetonitrile/50% water mixture.

Electrode Preparation. A gold wire (0.5 mm diameter, 99.999%, Alfa Aesar, MA) was cleaned by reflux in nitric acid (70%) at 130 °C for 2 h and then washed with deionized water (>18 MΩ·cm). The wire was sealed in a soft-glass capillary tube with the tip exposed. The tip of the gold wire was heated to form a ball. The gold ball was reheated in a flame until glowing, then slowly cooled, and finally quenched in deionized water. This annealing process was repeated more than 15 times until a smooth ball electrode was obtained. The area of the electrode was determined electrochemically[51] and found to be typically ~0.1 cm^2.

Self-Assembled Monolayer (SAM) Preparation. Self-assembled monolayers were prepared by incubating gold ball electrodes in 1 mL of a 20 μM PNA solution under the conditions specified in Table 1. After incubation the gold electrodes were washed with nanopure water and directly used in the electrochemical studies.

Evidence of ferrocene decomposition by cyclopentadiene loss was observed for the PNA oligomers if the incubation solutions were kept in light for several days. However, MALDI-ToF

characterization of the PNA SAMs (SAMDI-ToF)[52] showed no evidence of ferrocene decomposition after incubation at 30−40 °C for 42−48 h (see Supporting Information). After SAM preparation under the conditions described here, the electrodes could be kept in nanopure water, and electrochemical experiments could be performed more than 10 days after incubation without significant changes in the response.

Electrochemical Measurements. Cyclic voltammetry was carried out on a CH Instrument electrochemical analyzer 618B (Austin, TX). The three-electrode electrochemical cell consisted of an Ag/AgCl (3 M KCl) reference electrode, a platinum wire as counter electrode, and a SAM-coated gold ball electrode as the working electrode. All experiments were performed in 1 M $NaClO_4$ (pH = 7−8) aqueous electrolyte solution at room temperature. The uncompensated solution resistance was measured by ac impedance and found to be less than 5 Ω, indicating that the *iR* drop was not important for these measurements. The coverage of the PNA−ferrocene SAM was calculated by integrating the charge under the voltammetric peaks.

Atomic Force Microscopy (AFM). Atomic force microscopy was carried out on a Molecular Imaging PicoPlus (Tempe, AZ) instrument. A tapping mode silicon cantilever AFM tip (NSC16, resonant frequency 170 kHz, force constant 40 N/m, MikroMasch, Estonia) was used. AFM experiments were done in ambient at room temperature.

The Au bead electrode was made by melting a 0.8 mm Au wire (99.999%, Alfa Aesar, MA) in a hydrogen flame. Prior to the experiments the substrate was cleaned by immersion in hot "piranha" solution (1:3 H_2O_2 and 98% H_2SO_4) in ambient conditions at room temperature for 1 h. **(***Caution! The piranha solution is a very strong oxidizing agent and extremely dangerous. Eye protection and gloves should be used during handling.***)** After each step the sample was rinsed by sonication in deionized water. After cleaning, the crystal was annealed in a hydrogen flame and allowed to cool in air. The ∼2.6 mm diameter bead displayed numerous facets of ∼0.5 mm diameter, with predominant (111) orientation.

Ellipsometry and Contact Angle. The molecules were self-assembled to form a monolayer thick film on evaporated gold slides (EMF Corp, Ithaca, NY). The Au slides were 0.7 in. × 0.3 in. × 0.062 in. in size and consisted of about 100 nm Au over a 50 nm thick Ti binder layer on float glass. The gold slides were cleaned by immersion in "piranha" solution for 2 min and then rinsed by a large amount of deionized water followed by ethanol. They were subsequently dried under nitrogen. For SAM formation, the Au slides were incubated in 1.0 mL of a 20 μM PNA solution under the conditions specified in Table 1. After incubation, these SAM-coated gold slides were rinsed vigorously with ethanol and water and dried under nitrogen. The thickness was measured by a Gaertner L-117 Null ellipsometer, and the contact angle with water was measured on the same gold slides using a home-built goniometer system.

Background

The Electron-Transfer Rate Constant.[53−62] In the nonadiabatic limit, the electron-transfer rate constant k_{et} is given by the Fermi golden rule expression

$$k_{et} = \frac{2\pi}{\hbar}|V|^2 \mathrm{FCWDS} \tag{1}$$

Equation 1 describes the rate constant for a nonadiabatic transition between two states, which have an electronic coupling magnitude of $|V|$. FCWDS is the Franck−Condon weighted density of states, which accounts for the effect of nuclear coordinates on the rate constant. If the Gibbs reaction free energy (ΔG) is smaller than the reorganization energy λ of the reaction (normal regime) and if high-frequency vibrational modes of the donor and acceptor do not contribute significantly to the reorganization energy, the FCWDS can be written as

$$\mathrm{FCWDS} = \frac{1}{\sqrt{4\pi\lambda k_B T}} \exp\left[-\frac{(\lambda + \Delta G)^2}{4\lambda k_B T}\right] \tag{2}$$

The reorganization energy λ encompasses an inner-sphere contribution λ_{in}, which is associated with the internal coordinates of the redox species, and an outer-sphere component λ_{out}, which is dominated by the solvent polarization. For the ferrocene/ferrocenium redox couple the λ_{out} term is dominant, and the reorganization energy in water is reported to lie between 0.7 and 0.96 eV.[62,63]

For electron transfer at an electrode, eqs 1 and 2 must be generalized to consider the distribution of electronic states that are available in the solid. For an electron at energy ϵ in the electrode, the free energy of reaction is given by

$$\Delta G = (\epsilon_F - \epsilon) + e\eta \tag{3}$$

where η is the overpotential and ϵ_F is the Fermi level of the electrode. Substitution of eq 3 into eq 2 generates

$$k_{red}(\epsilon,\eta) = \frac{2\pi}{\hbar}|V|^2 \frac{1}{\sqrt{4\pi\lambda k_B T}} \exp\left[-\frac{(\lambda + (\epsilon_F - \epsilon) + e\eta)^2}{4\lambda k_B T}\right] \tag{4}$$

The total rate constant for reduction requires integration over all electronic states of the solid, so that

$$k_{red}(\epsilon,\eta) = \frac{2\pi}{\hbar}|V|^2 \frac{1}{\sqrt{4\pi\lambda k_B T}} \int_{-\infty}^{\infty} \rho(\epsilon) \exp\left[-\frac{(\lambda + (\epsilon_F - \epsilon) + e\eta)^2}{4\lambda k_B T}\right] f(\epsilon)\, d\epsilon \tag{5}$$

where $\rho(\epsilon)$ is the density of electronic states of the electrode (often an energy-independent average value is used) and $|V|$ is assumed to be independent of energy. $f(\epsilon)$ is the Fermi−Dirac distribution law

$$f(\epsilon) = \frac{1}{1 + \exp[(\epsilon - \epsilon_F)/k_B T]} \tag{6}$$

An expression similar to eq 5 can be written for the oxidation rate constant

$$k_{ox}(\epsilon,\eta) = \frac{2\pi}{\hbar}|V|^2 \frac{1}{\sqrt{4\pi\lambda k_B T}} \int_{-\infty}^{\infty} \rho(\epsilon) \exp\left[-\frac{(\lambda + (\epsilon_F - \epsilon) - e\eta)^2}{4\lambda k_B T}\right] [1 - f(\epsilon)]\, d\epsilon \tag{7}$$

The electron-transfer rate constants have been obtained by measuring the shift in the faradaic current peak potential as a function of voltage scan rate in cyclic voltammetry experiments and fitting of the data by the Marcus model. Equations 6 and 7 were used to create working curves of peak shift vs $\log_{10}$(scan rate/k^0) for specific values of λ at room temperature.[58] Those working curves were used to fit the experimental data and obtain the standard electrochemical rate constant k^0. See ref 58 for more details about this procedure.

Results

Characterization of PNA Monolayers. *Contact Angle Measurements.* The static contact angles measured for the PNA

TABLE 2: Ellipsometric Thickness, Calculated Length, and Contact Angle of PNA Molecules

molecule	ellipsometric thickness (nm)	calcd length of PNA (nm)	contact angle with H_2O (deg)
Cys-T3-Fc	1.4 ± 0.1	1.95	53 ± 2
Cys-T4-Fc	1.4 ± 0.1	2.30	47 ± 1
Cys-T5-Fc	1.3 ± 0.1	2.65	41 ± 1
Cys-T6-Fc	2.1 ± 0.1	3.00	40 ± 1
Cys-T7-Fc	2.3 ± 0.1	3.35	35 ± 1

SAMs with water are between 35° and 53° (Table 2), and they decrease with the increasing length of the PNA, which means that the hydrophilicity of the exposed surface increases with the PNA length. Because the thymines are hydrophilic and ferrocene is hydrophobic, the increase in hydrophilicity with the PNA length suggests that the thymines of the PNA oligomers are solvent accessible and the monolayer is not compact.

Ellipsometry Studies. Ellipsometry determines the film thickness by measuring the change in light polarization upon reflection from the surface. The thickness determination requires knowledge of the refractive index of the SAM. The refractive index of a PNA SAM has not been reported yet. Therefore, in this study, we have used a refractive index of 1.6, which is between the refractive indices of 1.57 and 1.7 reported for protein and DNA SAMs, respectively.[64−66] Any difference between the actual refractive index of a PNA SAM and 1.6 will cause a systematic error in the calculated thickness value, but it will not affect the trend observed for the change in thickness with the length of the PNA. The PNA SAM thicknesses, which have been obtained in this way, are compared with the calculated lengths of different PNA molecules in Table 2. These molecular lengths have been estimated by adding characteristic lengths for the cysteine (4 Å), the ferrocene (5 Å), and each PNA base (3.5 Å).[67]

If the SAM was highly compact and the PNA strands were fully extended, then the calculated lengths and the ellipsometrically determined film thicknesses would agree, for each PNA oligomer. In contrast, the ellipsometrically determined film thickness was less than the calculated length of the fully extended molecules (Table 2), and no systematic change of the SAM film thickness with the number of base pairs is evident. In order to understand the ellipsometric results better, the PNA SAMs were modeled in two different ways.

In the first model, the PNA SAMs were assumed to be compact, and all the PNA oligomers were assumed to be tilted on the surface at some angle from the surface normal. On the basis of this model, we determined by simple geometry an average tilt angle from the measured film thickness of 43 ± 4°, 51 ± 3°, 62 ± 3°, 46 ± 3°, and 47 ± 3° from Cys-T3-Fc to Cy-T7-Fc, respectively. These angles are relatively large when compared to the tilt angle of alkanethiol,[68,69] and there is no trend of the angles with the PNA length.

In the second model, the PNA SAMs were assumed to consist of two different phases that differed in thickness, namely a "lying-down" phase and a "standing-up" phase. The "standing-up" molecules were assumed to be oriented perpendicular to the surface, i.e., the PNA's backbone axis is oriented along the surface normal, and the "lying-down" molecules were assumed to be parallel to the Au surface, i.e., the backbone axis is perpendicular to the surface normal. The thickness of the "lying-down" molecules was taken as 0.5 nm, and the thickness of the "standing-up" molecules was taken to be the calculated length given in Table 2. The average thickness was computed as a weighted sum of the thickness for the "lying-down" molecules and the "standing-up" molecules. Equating the ellipsometric thickness to the average thickness allowed the percentage of each phase to be determined. The percentage of the "lying-down" phase was found to be 36 ± 5% for Cys-T3-Fc, 48 ± 4% for Cys-T4-Fc, 64 ± 6% for Cys-T5-Fc, 38 ± 4% for Cys-T6-Fc, and 38 ± 5% for Cys-T7-Fc. These percentages correspond to the geometric area of the surface that is covered by the "lying-down" phase and not the percentages of the PNA oligomers in each phase. If the "standing-up" molecules can be approximated as cylinders with a radius r of 0.49 nm[70] and height equal to the calculated length of the PNA, then the circular footprint of the molecules in the "standing-up" phase is $\pi r^2 = 0.75$ nm^2 and the rectangular footprint of molecules in the "lying-down" phase is $2rh = 0.98h$ nm^2. Using the ellipsometric fractions and this model, the percentage of the "lying-down" molecules are 14 ± 2% for Cys-T3-Fc, 16 ± 1.4% for Cys-T4-Fc, 19 ± 2% for Cys-T5-Fc, 10 ± 1% for Cys-T6-Fc, and 9 ± 1% for Cys-T7-Fc.

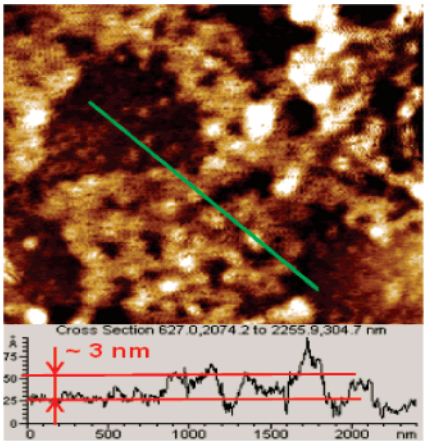

Figure 2. Tapping mode AFM topography image (3 μm × 3 μm) is shown for Cys-T6-Fc monolayer, collected in ambient at room temperature.

AFM Studies. Tapping mode atomic force microscopy was performed on a Cys-T6-Fc SAM formed on a (111) facet of a large gold bead. Note that the Au beads used for the AFM studies had an area which is about five times larger than the area of the Au ball electrodes used for electrochemistry. The AFM topography image in Figure 2 shows two distinct regions, with a significant height difference of about 3 nm. The calculated length of a fully extended Cys-T6-Fc is about 3 nm. This result supports the idea that a "standing-up" phase and a "lying-down" phase coexist on the Au surface. Analysis of multiple AFM images revealed that 52 ± 10% of the total area was occupied by a "lying-down" phase, which is somewhat larger than the 38 ± 4% value obtained from the ellipsometry measurements.

Electrochemical Characterization. This section describes the electrochemical manifestations of the PNA SAMs grown by incubating gold electrodes first at room temperature and then at higher temperature (35−40 °C).

Initial attempts to grow ss-PNA SAMs by incubation of the electrodes with a 20 μM solution of PNA in pH = 7, 10 mM phosphate buffer at room temperature for up to 48 h generated SAMs with low surface coverage of 50 ± 3 to 56 ± 5 pmol/cm^2, compared to the maximum expected surface coverage of 300 pmol/cm^2 for Cys-Tn-Fc,[70] where $n = 4-6$. The electron-transfer rate constants for these films were $k^0 = 1830 \pm 60$, 1100 ± 500, and 630 ± 30 s^{-1} for Cys-T4-Fc, Cys-T5-Fc, and Cys-T6-Fc, respectively. Given the poor surface coverage, it is possible that the PNA molecules were "lying down" on the surface. The weak length dependence may reflect a change in the average distance between the gold electrode and the ferrocene due to packing in the film. A similar high transfer

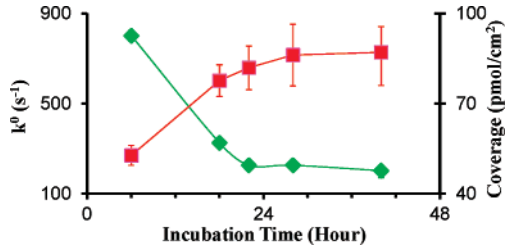

Figure 3. Electron-transfer rate (diamond symbols) and coverage (square symbols) for Cys-T4-Fc SAMs are plotted as a function of the incubation time at 35 °C.

rate was reported by Anne et al.[71] for thymine (T) containing single-stranded DNA molecules lying flat on gold surfaces.

Higher coverage and more compact films have been formed by incubating electrodes in PNA solutions at 35 °C. The surface coverage, which increased with the incubation time, was measured by integrating the charge passed in voltammograms; the growth of the Cys-T4-Fc SAM was complete in 22−28 h (Figure 3). Simultaneously, the measured electron-transfer rate constant, k^0, decreased with the increasing incubation time for a Cys-T4-Fc film, which suggests an increase in the fraction of PNA molecules that "stand up". In this case the charge transfer would take place by tunneling through the PNA rather than directly through space from ferrocene to the Au surface, which would dominate for PNA molecules that are "lying down". No significant change in coverage of Cys-T4-Fc SAMs was found by elevating the incubation temperature from 35 to 40 °C.

Although the optimized conditions lead to more compact films, it was not possible to make films in which all of the PNA molecules were "standing up" on the surface. For the oligomers Cys-T5-Fc, Cys-T6-Fc, and Cys-T7-Fc the presence of two different phases, namely "lying-down" and "standing-up" molecules, was observed by voltammetry. If the potential scan speed is slow enough in a voltammetry experiment, electrochemical reversibility can be achieved. For a reversible process, the full width at half maximum (fwhm) of the peaks is ~90.6 mV and the voltammetric peak maxima appear at the formal potential (E^0) of the redox probe. As the potential scan speed is increased and becomes fast compared to the electron-transfer rate, the voltammetric peak maxima shift away from the formal potential. If the electron-transfer rates of the "lying-down" and "standing-up" phases are different enough, their peaks shift by a different amount for a given scan speed and can be distinguished.

Figure 4 shows three representative voltammograms for Cys-T6-Fc. The voltammogram taken at a 20 mV/s scan speed shows a broad peak (200 mV fwhm) and a peak maximum that is shifted from the formal potential of ferrocene (panel A). The voltammogram at 80 mV/s scan speed shows two peaks: one which appears to be nearly reversible and one in which the peak maxima are strongly displaced from each other (panel B). The voltammogram taken at 1 V/s scan speed shows a sharp peak with a 102 mV fwhm and peak maxima close to the formal potential of the ferrocene (panel C).

These data can be understood in terms of two distinct populations of Cys-T6-Fc coexisting on the gold surface. One population has a fast electron-transfer rate, presumably a "lying-down" species in which the ferrocene is near the gold electrode. The second population has a slow electron-transfer rate, presumably a "standing-up" species in which electron transfer occurs through the PNA. At slow scan speeds, both populations undergo electron transfer. As the scan speed is increased, the peaks for the slow population shift and decrease in amplitude

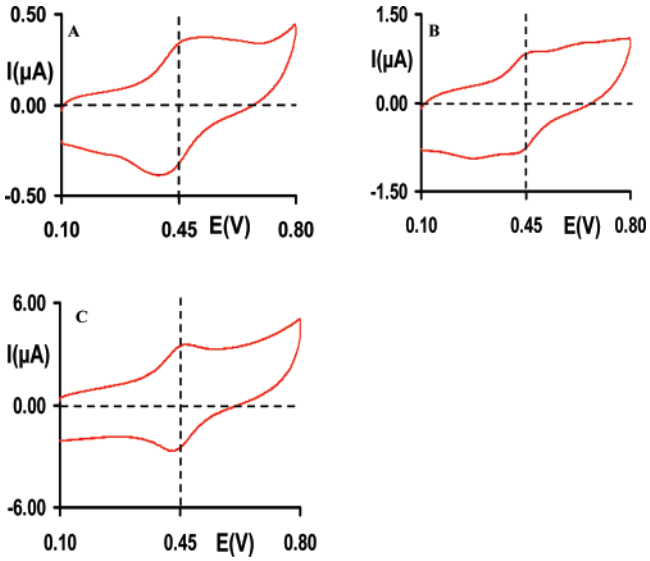

Figure 4. Three cyclic voltammograms are shown for Cys-T6-Fc SAM at scan rate (A) 20 mV/s, (B) 80 mV/s, and (C) 1 V/s. The vertical dashed line marks the formal potential of ferrocene.

until they are no longer evident in the potential window. If the scan speed is high enough, the "standing-up" species do not undergo electron transfer. Panel C corresponds to this latter case, in which the scan speed is slow compared to the electron-transfer rate for the "lying-down" species but is fast compared to the electron-transfer rate of the "standing-up" species. Consequently, the voltammogram looks nearly ideal and corresponds to reduction and oxidation of the "lying-down" species only.

This interpretation of the electrochemical behavior was corroborated by the analysis of the total charge passed through the film. At the 20 mV/s scan speed (panel A) the total charge is 1.5 μC, whereas at 1 V/s the total charge is only 0.14 μC. Hence at 20 mV/s, the slow species dominates the response and the peak maxima are shifted. Less charge is passed at the higher scan speed because only the "lying-down" species undergo electron transfer. For this particular Cys-T6-Fc film, the percentage of "lying-down" molecules was found to be 9.3% from the charge passed, corresponding to 14.5 pmol/cm^2. This percentage of "lying-down" and "standing-up" species is similar to that found according to the second model applied to the ellipsometry experiments.

A similar electrochemical behavior attributable to the coexistence of "lying-down" and "standing-up" molecules was observed for Cys-T5-Fc and Cys-T7-Fc. In the cases of Cys-T3-Fc and Cys-T4-Fc, the presence of two different phases was not observed, and a possible explanation is described in the Discussion and Conclusions section (vide infra).

Measurement of k^0 for the "Standing-Up" Subpopulation. The standard heterogeneous electrochemical rate constant was determined by first making the "lying-down" subpopulation electroactively silent and then studying the scan speed dependence of the "standing-up" phase. In this way, the "lying-down" phase does not interfere with the rate constant determination.

The ferrocenium ion can exchange one of its cyclopentadienyl rings for an anion of the electrolyte solution (Figure 5).[53] This exchange is slow and not significant when the electrolyte solution contains perchlorate but it is much faster with chloride or sulfate anions.[53] By exploiting the difference in the oxidation kinetics for the "lying-down" and "standing-up" species, it is possible to preferentially react the "lying-down" species with chloride ion.

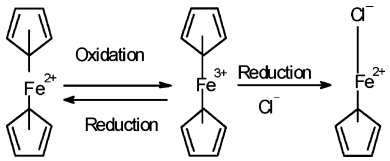

Figure 5. Ferrocene reaction during cyclic voltammetry cycles.

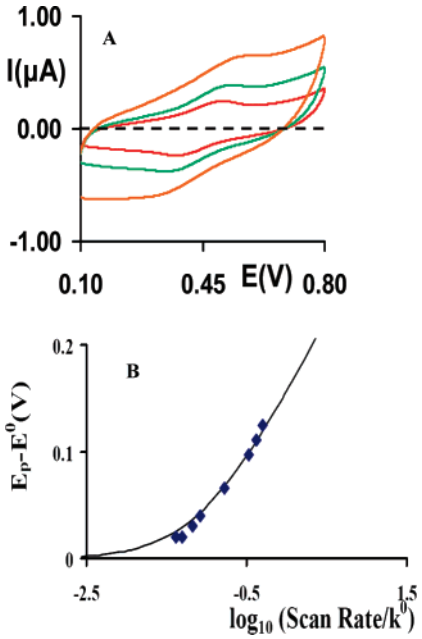

Figure 6. (A) Cyclic voltammograms are shown for Cys-T6-Fc SAM at scan rates 5 mV/s (red), 10 mV/s (green), and 20 mV/s (orange). (B) A fitting curve is plotted for the determination of electron-transfer rate of Cys-T6-Fc SAM. The diamond symbols represent the experimentally determined points, and the solid line represents the best fit theoretical curve.

The protocol for preferentially destroying the "lying-down" species by the reaction with chloride was to scan the PNA SAM-coated electrode to potentials between 0.35 and 0.65 V in 1 M NaCl solution at scan rates of 1 V/s for Cys-T6-Fc and Cys-T7-Fc and at 10 V/s for Cys-T5-Fc until the voltammetric peak of the "lying-down" species disappeared. Scanning at higher scan speed did not destroy the ferrocene of the "standing-up" species because oxidation of the "standing-up" ferrocene is too slow. Subsequent to this process, the NaCl electrolyte was replaced with a $NaClO_4$ electrolyte, and voltammetry was used to determine the electron-transfer rate constant k^0 for the "standing-up" species without interference.

The results of a voltammetry study of the "standing-up" species of the Cys-T6-Fc films are shown in Figure 6, after the redox species in the "lying-down" phase were destroyed. The voltammograms in Figure 6A show that as the voltammetric scan speed increases, the voltammetric peak maxima shift away from the formal potential. Figure 6B plots the dependence of the oxidation peak potential on the scan speed and compares it to the prediction of the Marcus theory,[55,56] in which the electron-transfer rate k^0 was used as an adjustable parameter and the reorganization energy for ferrocene was taken to be 0.8 eV.[58] The voltammograms and fitting curves of other PNA SAMs are shown in the Supporting Information.

The k^0 values determined from the oxidation and reduction waves were different, with those for reduction being consistently 1.5 times larger than those for oxidation (Table 3). It is likely that this asymmetry in the electron-transfer rate arises from ion pairing of the surface-bound ferrocenium with the anion of the electrolyte solution, as reported by others.[72] Alternatively, interactions between redox centers can cause such asymmetries.[61] For simplicity, the discussion focuses on the oxidation waves as others have done for alkanethiol−ferrocene assemblies.[58,73]

TABLE 3: Electron-Transfer Rate and Coverage for the "Standing-Up" Population of PNA SAMs

molecule	k^0 (s^{-1})	coverage ($pmol/cm^2$)	fwhm[a] (mV)	no. of trials
Cys-T3-Fc	2000 ± 200	89 ± 8	115 ± 3 (1 V/s)	5
Cys-T4-Fc	200 ± 20	87 ± 7	116 ± 3 (0.1 V/s)	9
Cys-T5-Fc	3.0 ± 0.5	47 ± 3	106 ± 4 (0.01 V/s)	3
Cys-T6-Fc	0.14 ± 0.03	140 ± 60	129 ± 4 (0.005 V/s)	5
Cys-T7-Fc	0.018 ± 0.002	80 ± 10	188 ± 6 (0.005 V/s)	4

[a] The scan speeds at which fwhms are calculated are reported in parentheses.

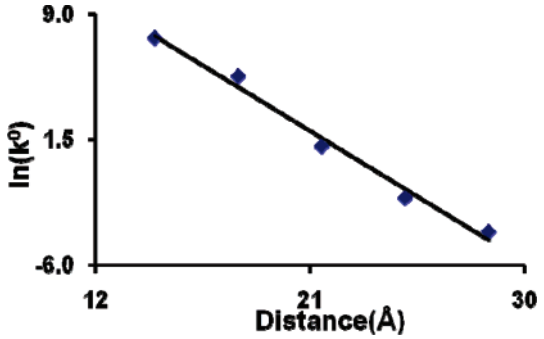

Figure 7. Electron-transfer rate of PNA molecules are plotted as a function of the distance between gold electrode and ferrocene (blue diamond symbols) (error bars are smaller than symbols). The solid line represents the best fit line used for the determination of the tunneling decay constant (β) for thymine (T) containing single-stranded PNA molecules.

The full width at half-maximum (fwhm) for different PNA molecules are listed in Table 3. For Cys-T6-Fc and Cys-T7-Fc, electrochemical reversibility was not achieved even at the slowest scan speed because the electron-transfer rates were very slow. Simulations of the voltammograms for Cys-T6-Fc and Cys-T7-Fc at a scan speed of 0.005 V/s gave a fwhm of 106 mV for Cys-T6-Fc and 124 mV for Cys-T7-Fc. As Table 3 shows, the experimental fwhm for shorter PNA oligomers are somewhat broader than the ideal limit of a homogeneous film (90.6 mV). This result may be attributed to interaction between redox centers[74] or to the inhomogeneity of the films.[61]

Distance Dependence of k^0 through PNA. The electron-transfer rate constant for the "standing-up" phase decreases as the number of thymine nucleotides in the PNA chain increases. The exponential dependence revealed by Figure 7 is consistent with a charge transfer that occurs by a superexchange mechanism.[9−19] The slope of the line gives a tunneling decay constant of $\beta = 0.86 \pm 0.04$ Å^{-1} ($\beta = 3.0 \pm 0.1$/base),[75] which is comparable to the tunneling decay constants reported for alkanethiols[63,73,76−78] and for peptides.[79,80]

Dicussion and Conclusions

In this work single-stranded peptide nucleic acid oligomers consisting of thymine bases were self-assembled on a gold surface. In order to obtain a high coverage and compact films, the assembly was performed at 35−40 °C. The SAM was

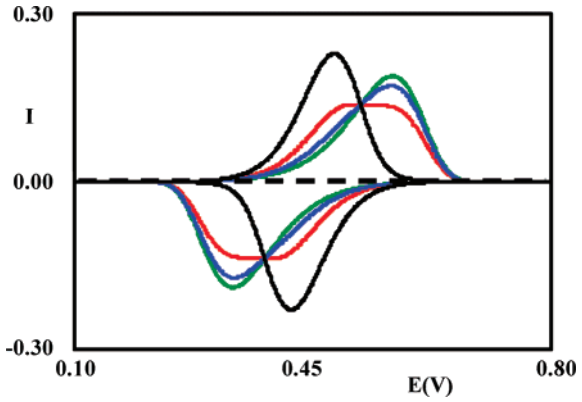

Figure 8. Simulated voltammograms obtained for four different cases at scan rate 100 V/s. Solid green and black voltammograms are for species having $k^0 = 200\ s^{-1}$ and $k^0 = 1800\ s^{-1}$, respectively. The blue and red voltammograms are for 9:1 ratio and 7:3 ratio of two species, having $k^0 = 200\ s^{-1}$ and $k^0 = 1800\ s^{-1}$, respectively.

characterized by SAMDI-ToF mass spectrometry, cyclic voltammetry, atomic force microscopy, contact angle, and ellipsometry measurements. Electrochemistry detected two distinct populations of molecules in the PNA SAM, one consisting of "lying-down" molecules with a fast electron-transfer rate and the other of "standing-up" molecules with a slow electron-transfer rate. The AFM studies of Cys-T6-Fc also revealed that ss-PNA SAM is composed of "lying-down" and "standing-up" species. The percentage of "lying-down" molecules varied with the number of T bases of the PNA. According to cyclic voltammetry, percentages of the "lying-down" molecules were 27 ± 5%, 10 ± 3%, and 9 ± 2% for Cys-T*n*-Fc, where $n = 5-7$, respectively, and according to ellipsometry the percentages of "lying-down" molecules were 14 ± 2%, 16 ± 1%, 19 ± 2%, 10 ± 1%, and 9 ± 1% for Cys-T*n*-Fc, where $n = 3-7$, respectively.

In contrast to Cys-T5-Fc, Cys-T6-Fc, and Cys-T7-Fc, the presence of two subpopulations of ferrocene was not apparent in the voltammetry of Cys-T3-Fc and Cys-T4-Fc assemblies. Nevertheless, the ellipsometry measurements suggested that some of the PNA molecules were "lying down" on these surfaces. The failure to observe two phases in the voltammetry of Cys-T3-Fc and Cys-T4-Fc, could be caused by the fact that the rate constants for the "lying-down" and "standing-up" phases are not different enough to generate distinguishable peaks in cyclic voltammetry. Presumably, the electron-transfer rates of the "standing-up" species of Cys-T3-Fc and Cys-T4-Fc are much higher than that of Cys-T5-Fc, Cys-T6-Fc, or Cys-T7-Fc, and thus the voltammetric peak starts to shift at higher scan speeds; this makes the analysis more difficult because the rate of the "standing-up" phase is closer to the rate of the "lying-down" phase.

Simulated voltammograms[81] were used to assess this effect (Figure 8). If two species are present at a 9:1 ratio (blue voltammogram) and have a significantly different k^0 (9 times), the peak for the majority species ("standing up") dominates the response over the minority ("lying down"); i.e., the voltammetric peaks remain at the same position where the majority species ("standing-up", green voltammogram) have a peak, even if 10−15% molecules have a faster electron-transfer rate. These simulated voltammograms do not consider background charging; however, the background charge was relatively low for the Cys-T3-Fc and Cys-T4-Fc films (see Supporting Information). However, the red voltammogram of Figure 8 shows that if the ratio is increased to 7:3, then a peak maximum appears in between the majority ("standing-up") (green voltammogram) and minority ("lying-down") species (black voltammogram). The simulated voltammograms imply that if "lying-down" molecules represent up to 15% of all molecules, then k^0 measured for the mixture coincides with the one for the majority species, but if the minority species ("lying down") is 30% or more, then the apparent k^0 is lower than that for the majority species. The ellipsometry data analysis suggest that for Cys-T3-Fc and Cys-T4-Fc the percentage of "lying-down" species is below 20%.

These findings should be contrasted with those of Martin-Gago and co-workers, who successfully formed a densely packed peptide nucleic acid (PNA) SAM by incubation of Au surfaces at room temperature.[42−44] The difference may be due to the fact that the PNA oligomers used in their studies contained a 3 nm linker between the PNA and the cysteine. Unfortunately, such long linkers are incompatible with the distance-dependent charge-transfer studies pursued here because they slow down the charge-transfer rate.

By creating compact films and chemically destroying the "lying-down" species, the slower electron-transfer rate constant of the "standing-up" species could be measured. The distance-dependent charge transfer of the thymine (T) containing PNA SAMs had a tunneling decay constant similar to that of peptide linkages,[79,80] $\beta = 0.86 \pm 0.04\ Å^{-1}$. Using this value and extrapolating to zero distance, i.e., to contact between ferrocene and the electrode, provides a maximum electron-transfer rate constant of $5.8 \times 10^8\ s^{-1}$. This value is similar to that obtained by Smalley et al.[63] for ferrocene-terminated alkanethiol ($6 \times 10^8\ s^{-1}$). Using the semiclassical Marcus theory, a contact electronic coupling between the donor and acceptor of about $69\ cm^{-1}$ is obtained. This value is small enough that the electron transfer can be reasonably modeled as nonadiabatic.

The electron-transfer rate constant measured for the thymine-containing single-stranded PNA molecules is slower than that reported for duplex DNA.[29−31,33] This difference could arise from the fact that the base stacking,[82] which is important for long-range charge transfer, is weaker in ss-PNA compared to ds-DNA. It is worth noting that such a conclusion cannot be drawn based on the present study but it requires a detailed systematic study, which is underway in our laboratory. In the case of DNA, long-range charge transfer has been explained by a hopping mechanism;[20−25] i.e., thermal oxidation of the guanine (G) or adenine (A) bases competes with the tunneling when the bridge between the donor and acceptor is long.[25] Thymine is more difficult to oxidize so that the tunneling pathway remains dominant for longer oligomers than what one would expect if G or A bases were present. Charge transport in the short thymine PNAs used here appears to operate by a single-step superexchange-mediated tunneling mechanism.

Acknowledgment. D.H.W., C.A., and E.B. acknowledge support from the U.S. National Science Foundation (CHE 0628169). A.P. thanks Dr. Andrew M. Napper and Dr. Jianjun Wei for useful discussions during this study. We thank Violeta Marin for her expert help and advice with the SAMDI-ToF studies. We also thank Prof. David N. Beratan for useful discussions during this study. C.A. acknowledges support by the Sloan Foundation and the Camille and Henry Dreyfus Foundation.

Supporting Information Available: Cyclic voltammograms, fitting curves of different PNA molecules, MALDI-ToF, and SAMDI-ToF. This material is available free of charge via the Internet at http://pubs.acs.org.

References and Notes

(1) Schwartz, D. K. *Annu. Rev. Phys. Chem.* **2001**, *52*, 107−137.

(2) Ulman, A. *Chem. Rev.* **1996**, *96*, 1533−1554.

(3) Jortner, J.; Ratner, M. A. *Molecular Electronics;* Blackwell: London, 1997.

(4) Kumar, A.; Biebuyck, H. A.; Whitesides, G. M. *Langmuir* **1994**, *10*, 1498−1511.

(5) Revell, D. J.; Knight, J. R.; Blyth, D. J.; Haines, A. H.; Russell, D. A. *Langmuir* **1998**, *14*, 4517−4524.

(6) Bain, C. D.; Evans, S. D. *Chem. Br.* **1995**, *31*, 46.

(7) Donhauser, Z. J.; Mantooth, B. A.; Kelly, K. F.; Bumm, L. A.; Monnell, J. D.; Stapleton, J. J., Jr; D. W. P.; Rawlett, A. M.; Allara, D. L.; Tour, J. M.; Weiss, P. S. *Science* **2001**, *292*, 2303−2307.

(8) Prime, K. L.; Whitesides, G. M. *Science* **1991**, *252*, 1164−1167.

(9) Degama, A. A. S. *Theor. Chim. Acta* **1985**, *68*, 159.

(10) Evenson, J. W.; Karplus, M. *Science* **1993**, *262*, 1247−1249.

(11) Gehlen, J. N.; Daizadeh, I.; Stuchebrukhov, A. A.; Marcus, R. A. *Inorg. Chim. Acta* **1996**, *243*, 271−282.

(12) Goldman, C. *Phys. Rev. A* **1991**, *43*, 4500.

(13) Harden, M. M. *J. Chem. Phys.* **1961**, *35*, 508−515.

(14) Joachim, C.; Ratner, M. A. *Nanotechnology* **2004**, *15*, 1065.

(15) Magoga, M.; Joachim, C. *Phys. Rev. B* **1997**, *56*, 4722.

(16) Priyadarshy, S.; Risser, S. M.; Beratan, D. N. *J. Phys. Chem.* **1996**, *100*, 17678−17682.

(17) Ratner, M. A. *J. Phys. Chem.* **1990**, *94*, 4877−4883.

(18) Reimers, J. R.; Hush, N. S. *J. Photochem. Photobiol., A* **1994**, *82*, 31−46.

(19) Remacle, F.; Levine, R. D. *J. Phys. Chem. B* **2001**, *105*, 2153−2162.

(20) Berlin, Y. A.; Burin, A. L.; Ratner, M. A. *Chem. Phys.* **2002**, *275*, 61−74.

(21) Berlin, Y. A.; Hutchison, G. R.; Rempala, P.; Ratner, M. A.; Michl, J. *J. Phys. Chem. A* **2003**, *107*, 3970−3980.

(22) Giese, B. *Annu. Rev. Biochem.* **2002**, *71*, 51−70.

(23) Jortner, J.; Bixon, M.; Langenbacher, T.; Michel-Beyerle, M. E. *Proc. Natl. Acad. Sci. U.S.A.* **1998**, *95*, 12759.

(24) Li, X. Q.; Zhang, H.; Yan, Y. *J. Phys. Chem. A* **2001**, *105*, 9563−9567.

(25) Schuster, G. B. *Long-Range Charge Transfer in DNA I*; Top. Curr. Chem. Vols. 236 and 237; Springer: New York, 2004.

(26) Casero, E.; Darder, M.; Diaz, D. J.; Pariente, F.; Martin-Gago, J. A.; Abruna, H.; Lorenzo, E. *Langmuir* **2003**, *19*, 6230−6235.

(27) Herne, T. M.; Tarlov, M. J. *J. Am. Chem. Soc.* **1997**, *119*, 8916−8920.

(28) Zhang, R. Y.; Pang, D. W.; Zhang, Z. L.; Yan, J. W.; Yao, J. L.; Tian, Z. Q.; Mao, B. W.; Sun, S. G. *J. Phys. Chem. B* **2002**, *106*, 11233−11239.

(29) Hartwich, G.; Caruana, D. J.; de Lumley-Woodyear, T.; Wu, Y.; Campbell, C. N.; Heller, A. *J. Am. Chem. Soc.* **1999**, *121*, 10803−10812.

(30) (a) Liu, T.; Barton, J. K. *J. Am. Chem. Soc.* **2005**, *127*, 10160−10161. (b) Drummond, T. G.; Hill, M. G.; Barton, J. K. *J. Am. Chem. Soc.* **2004**, *126*, 15010−15011. (c) Kelley, S. O.; Barton, J. K. *Bioconjugate Chem.* **1997**, *8*, 31−37.

(31) Kelley, S. O.; Boon, E. M.; Barton, J. K. *Angew. Chem., Int. Ed.* **1999**, *38*, 941.

(32) Chahma, M.; Lee, J. S.; Kraatz, H.-B. *J. Electroanal. Chem.* **2004**, *567*, 283−287.

(33) Long, Y. T.; Li, C. Z.; Sutherland, T. C.; Chahma, M.; Lee, J. S.; Kraatz, H. B. *J. Am. Chem. Soc.* **2003**, *125*, 8724−8725.

(34) Egholm, M.; Buchardt, O.; Christensen, L.; Behrens, C.; Freier, S. M.; Driver, D. A.; Berg, R. H.; Kim, S. K.; Norden, B.; Nielsen, P. E. *Nature (London)* **1993**, *365*, 566−568.

(35) Egholm, M.; Nielsen, P. E.; Buchardt, O.; Berg, R. H. *J. Am. Chem. Soc.* **1992**, *114*, 9677−9678.

(36) Petersson, B.; Nielsen, B. B.; Rasmussen, H.; Larsen, I. K.; Gajhede, M.; Nielsen, P. E.; Kastrup, J. S. *J. Am. Chem. Soc.* **2005**, *127*, 1424−1430.

(37) Rasmussen, H.; Kastrup, J. S.; Nielsen, J. N.; Nielsen, J. M.; Nielsen, P. E. *Nat. Struct. Biol.* **1997**, *4*, 98−101.

(38) Rasmussen, H.; Liljefors, T.; Petersson, B.; Nielsen, P. E.; Kastrup, J. S. *J. Biomol. Struct. Dyn.* **2004**, *21*, 495−502.

(39) Franzini, R. M.; Watson, R. M.; Patra, G. K.; Breece, R. M.; Tierney, D. L.; Hendrich, M. P.; Achim, C. *Inorg. Chem.* **2006**, *45*, 9798−9811.

(40) Popescu, D. L.; Parolin, T. J.; Achim, C. *J. Am. Chem. Soc.* **2003**, *125*, 6354−6355.

(41) Watson, R. M.; Skorik, Y. A.; Patra, G. K.; Achim, C. *J. Am. Chem. Soc.* **2005**, *127*, 14628−14639.

(42) Briones, C.; Mateo-Marti, E.; Gomez-Navarro, C.; Parro, V.; Roman, E.; Martin-Gago, J. A. *Phys. Rev. Lett.* **2004**, *93*, 208103.

(43) Briones, C.; Mateo-Marti, E.; Gomez-Navarro, C.; Parro, V.; Roman, E.; Martin-Gago, J. A. *J. Mol. Catal. A: Chem.* **2005**, *228*, 131−136.

(44) Mateo-Marti, E.; Briones, C.; Roman, E.; Briand, E.; Pradier, C. M.; Martin-Gago, J. A. *Langmuir* **2005**, *21*, 9510−9517.

(45) Seidel, C. A. M.; Schulz, A.; Sauer, M. H. M. *J. Phys. Chem.* **1996**, *100*, 5541−5553.

(46) Azzam, R. M. A.; Bashara, N. M. *Ellipsometry and Polarized Light;* North-Holland Publishing Co.: Amsterdam, 1977.

(47) Tompkins, H. G. *A User's Guide to Ellipsometry;* Academic Press: New York, 1993.

(48) Anderson, G. W.; McGregor, A. C. *J. Am. Chem. Soc.* **1957**, *79*, 6180−6183.

(49) McKay, F. C.; Albertson, N. F. *J. Am. Chem. Soc.* **1957**, *79*, 4686−4690.

(50) Nielsen, P. E. *Peptide Nucleic Acids: Protocols and Applications;* Horizon Bioscience: Wymondham, UK, 2004.

(51) Sawyer, D. T.; Sobkowiak, A.; Roberts, J. L. *Experimental Electrochemistry for Chemists*; Wiley: New York, 1995.

(52) Patrie, S. M.; Mrksich, M. *Anal. Chem.* **2007**, *79*, 5878−5887.

(53) Finklea, H. O. In *Electroanalytical Chemistry*; Bard, A. J., Rubinstein, I., Eds.; Marcel Dekker: New York, 1996; Vol. 19, p 109.

(54) Khoshtariya, D. E.; Dolidze, T. D.; Zusman, L. D.; Waldeck, D. H. *J. Phys. Chem. A* **2001**, *105*, 1818−1829.

(55) Marcus, R. A. *J. Chem. Phys.* **1956**, *24*, 966−978.

(56) Marcus, R. A. *J. Chem. Phys.* **1965**, *43*, 679−701.

(57) Miller, C. J. *Physical Electrochemistry: Principles, Methods and Applications;* Rubinstein, I., Ed.; Marcel Dekker: New York, 1995; p 27.

(58) Napper, A. M.; Liu, H.; Waldeck, D. H. *J. Phys. Chem. B* **2001**, *105*, 7699−7707.

(59) Wei, J.; Liu, H.; Dick, A. R.; Yamamoto, H.; He, Y.; Waldeck, D. H. *J. Am. Chem. Soc.* **2002**, *124*, 9591−9599.

(60) Barbara, P. F.; Meyer, T. J.; Ratner, M. A. *J. Phys. Chem.* **1996**, *100*, 13148−13168.

(61) Bard, A. J.; Faulkner, L. R. *Electrochemical Methods; Fundamental and Applications*; Wiley: New York, 1980.

(62) Chidsey, C. E. D. *Science* **1991**, *251*, 919−922.

(63) Smalley, J. F.; Feldberg, S. W.; Chidsey, C. E. D.; Linford, M. R.; Newton, M. D.; Liu, Y.-P. *J. Phys. Chem.* **1995**, *99*, 13141−13149.

(64) Harrington, R. E. *J. Am. Chem. Soc.* **1970**, *92*, 6957−6964.

(65) Jung, L. S.; Campbell, C. T.; Chinowsky, T. M.; Mar, M. N.; Yee, S. S. *Langmuir* **1998**, *14*, 5636−5648.

(66) Wu, P. G.; Fujimoto, B. S.; Song, L.; Schurr, J. M. *Biophys. Chem.* **1991**, *41*, 217−236.

(67) The length of cysteine, ferrocene, and each PNA base has been calculated by CAChe software. Geometry has been optimized by the PM3 method.

(68) Ehler, T. T.; Malmberg, N.; Noe, L. J. *J. Phys. Chem. B* **1997**, *101*, 1268−1272.

(69) Porter, M. D.; Bright, T. B.; Allara, D. L.; Chidsey, C. E. D. *J. Am. Chem. Soc.* **1987**, *109*, 3559−3568.

(70) Assuming, that ssPNA has a radius similar to ssDNA, the radius of ssPNA is taken as 4.9 Å. Mucic, R. C.; Herrlein, M. K.; Mirkin, C. A.; Letsinger, R. L. *Chem. Commun.* **1996**, *4*, 555−557.

(71) Anne, A.; Demaille, C. *J. Am. Chem. Soc.* **2006**, *128*, 542−557.

(72) Rowe, G. K.; Creager, S. E. *Langmuir* **1991**, *7*, 2307−2312.

(73) Weber, K.; Hockett, L.; Creager, S. *J. Phys. Chem. B* **1997**, *101*, 8286−8291.

(74) Peng, Z.; Qu, X.; Dong, S. *J. Electroanal. Chem.* **2004**, *563*, 291−298.

(75) This error is a 2σ error in the slope obtained by a weighted linear least-squares fit and assuming no error in the distance values for the films.

(76) Carter, M. T.; Rowe, G. K.; Richardson, J. N.; Tender, L. M.; Terrill, R. H.; Murray, R. W. *J. Am. Chem. Soc.* **1995**, *117*, 2896−2899.

(77) Slowinski, K.; Chamberlain, R. V.; Miller, C. J.; Majda, M. *J. Am. Chem. Soc.* **1997**, *119*, 11910−11919.

(78) Sumner, J. J.; Weber, K. S.; Hockett, L. A.; Creager, S. E. *J. Phys. Chem. B* **2000**, *104*, 7449−7454.

(79) Sek, S.; Sepiol, A.; Tolak, A.; Misicka, A.; Bilewicz, R. *J. Phys. Chem. B* **2004**, *108*, 8102−8105.

(80) Tao, N. *J. Mater. Chem.* **2005**, *15*, 3260−3263.

(81) Simulated voltammograms are generated by CH Instruments (Austin, TX) software package. Background charge was not included in the calculation of these simulated voltammograms because this charge was relatively low for the Cys-T3-Fc and Cys-T4-Fc films (see Supporting Information).

(82) Jacobsen, E. N. *Comprehensive Organometallic Chemistry II*; Permagon: New York, 1995; Vol. 12, p 1097, and references therein.